ACSNANO
www.acsnano.org
ARTICLE

Freestanding Flag-Type Triboelectric Nanogenerator for Harvesting High-Altitude Wind Energy from Arbitrary Directions

Zhenfu Zhao,[†,§] Xiong Pu,[†,§] Chunhua Du,[†] Linxuan Li,[†] Chunyan Jiang,[†] Weiguo Hu,[*,†] and Zhong Lin Wang[*,†,‡]

[†]Beijing Institute of Nanoenergy and Nanosystems, Chinese Academy of Science, National Center for Nanoscience and Technology (NCNST), Beijing 100083, China

[‡]School of Materials Science and Engineering, Georgia Institute of Technology, Atlanta, Georgia 30332-0245, United States

Supporting Information

ABSTRACT: **Wind energy at a high altitude is far more stable and stronger than that near the ground, but it is out of reach of the wind turbine. Herein, we develop an innovative freestanding woven triboelectric nanogenerator flag (WTENG-flag) that can harvest high-altitude wind energy from arbitrary directions. The wind-driven fluttering of the woven unit leads to the current generation by a coupled effect of contact electrification and electrostatic induction. Systematic study is conducted to optimize the structure/material parameters of the WTENG-flag to improve the power output. This 2D WTENG-flag can also be stacked in parallel connections in many layers for a linearly increased output. Finally, a self-powered high-altitude platform with temperature/humidity sensing/telecommunicating capability is demonstrated with the WTENG-flag as a power source. Due to the light weight, low cost, and easy scale-up, this WTENG-flag has great potential for applications in weather/environmental sensing/monitoring systems.**

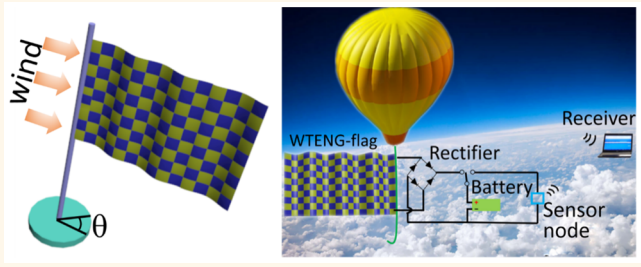

KEYWORDS: *triboelectric nanogenerator, wind energy, arbitrary direction, high-altitude platform*

Wind energy, as a clean and renewable energy source, is one of the most promising alternative solutions to the increasing threat of the global warming and energy crisis.[1,2] The conventional wind turbine has been long developed to harvest wind energy near the ground and has equipped wind power plants all over the world. However, the near-ground wind is highly dependent on the geography and weather. Recent studies have shown that these limitations can be eliminated by developing high-altitude wind power technology.[3−6] Compared with near-ground wind, the advantages of high-altitude wind energy include fast speed, wide distribution, high stability, and perenniality.[7] Meanwhile, high-altitude platforms (HAPs), situated at altitudes 17−22 km above the ground, have the capability of providing services and applications ranging from broadband wireless access,[8] navigation and positioning systems,[9] and remote sensing[10] to weather observation/monitoring systems.[11] For example, Google recently launched a project to provide a wireless network for remote areas using a balloon, named project loon. Current HAPs are mostly powered by batteries or engines, which limit their residence time at a high altitude due to recharging or refueling. Therefore, technologies for harvesting high-altitude wind energy are required to supply permanent power for HAPs. A conventional wind turbine is not suitable for this application, due to its large volume and weight and the high cost of manufacturing and installation.[2] To date, although various other prototypes have been examined to scavenge this energy, such as tethered airfoils,[6] ladder mills,[12] rotorcraft, and descending kites,[13] most of them are still in early stages and more innovative approaches are required.

Triboelectric nanogenerators (TENGs) have been recently invented as an effective way to harvest energy from our living environment (such as wind, sound, flowing water, human motion) based on the coupling of the triboelectric and electrostatic effects.[14−18] Efforts have been made to improve its electric output performance.[19−25] Until now, it has reached an output area power density of up to 500 W m^{-2} and a total energy conversion efficiency of up to 85%.[26] With its advantages of simple fabrication, excellent reliability, large output power, high efficiency, and low cost, the TENG has been intensively investigated for its promising applications in biomedical monitoring,[27] touch sensors,[28] human-interactive

Received: November 13, 2015
Accepted: January 7, 2016

DOI: 10.1021/acsnano.5b07157
ACS Nano XXXX, XXX, XXX−XXX

devices,[29] wearable electronics,[30,31] security surveillance, and healthcare monitoring.[32] Recently, flutter-driven TENGs harvesting wind energy have been developed, which are capable of lighting up tens of commercial light-emitting diodes (LEDs)[33] and powering a wireless sensor node.[34] However, the flutter-driven TENGs are usually constrained in one gas tube and interact with a counter rigid plate.[33−35] These structural designs make them unable to harvest wind energy from arbitrary directions. Moreover, their heavy weight also limits their applications in HAPs.

Herein, we report a lightweight and freestanding flag-type woven TENG (WTENG) that can scavenge wind energy from arbitrary directions. The working mechanism of the WTENG-flag is based on the interlaced interactions between Kapton film and a conductive cloth under wind-introduced fluttering of the flag. The output performance of the WTENG-flag has been optimized by systematically investigating the effects of the wind speeds and structural designs. Effects of environmental conditions (temperature and humidity) were also studied to confirm its suitability for high-altitude applications. The WTENG-flag was demonstrated to be capable of lighting up tens of commercial green LEDs brightly and powering a wireless temperature and humidity sensor node, which has remote telecommunication with a computer. Our study provides a promising approach for harvesting high-altitude wind energy and powering electronic devices for the applications of HAPs.

RESULTS AND DISCUSSION

The electricity generation by the TENG typically requires two steps, that is, contact electrification (or triboelectrification) and electrostatic induction. Mechanical energies of relative contact-separation motions or sliding motions can thus be converted into electricity in the external circuits. To harvest wind energy from arbitrary directions, a flag-type TENG is the ideal design, which, however, excludes the use of rigid sliding trails or hard substrate plates. Therefore, a WTENG-flag, as illustrated in Figure 1a, is designed to realize wind-driven relative contact-separation motions and thus the wind-to-electricity energy conversion. The WTENG-flag was woven by conductive belts of Ni-coated polyester textiles (Ni belts) and Kapton film-sandwiched Cu belts (KSC belts). In each woven unit, a gap was left between the two electrodes to allow the contact-separation motion driven by wind fluttering, as shown in the enlarged scheme in Figure 1a. All of the Ni belts were connected together as one electrode, while all of the sandwiched KSC belts were connected as the other. The Ni belts were fabricated by electroless plating of Ni film on commercial flexible polyester textiles. The nickel coating is conformal and covers both top and bottom sides of the polyester belts. The KSC belts were obtained by sealing both sides of the Cu foil with the Kapton film (20 μm thick), forming a sandwiched structure. Figure 1b shows a photo of the fabricated Ni belts and KSC belts (both are 1.5 cm wide and 30 cm long). Figure 1c is a photo of the WTENG-flag. The whole WTENG-flag is flexible and can be bent, folded, or twisted. Compared with other wind-harvested devices,[36,37] this WTENG-flag is much lighter (less than 15 g). Meanwhile, the used materials are low cost, and the whole fabrication is inexpensive and suitable for mass production. Figure S1 illustrates the scanning electron microscopy image of the Ni belts with a woven structure composed of polyester microwires. The surface of the polyester wires is fully covered by a

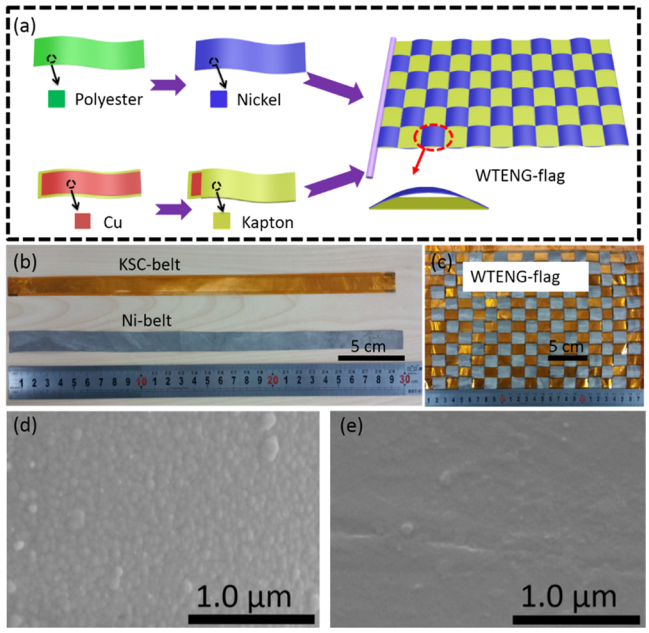

Figure 1. Fabrication of a woven TENG-flag (WTENG-flag). (a) Schematic illustration of the fabrication of WTENG-flag. (b) Optical image of Kapton film-sealed Cu belt (KSC belt) and conductive belt of Ni-coated polyester textiles (Ni belt). (c) Optical image of WTENG-flag composed of woven Ni belts and KSC belts. Scanning electron microscopy images of (d) one single polyester microwire coated with compact Ni nanoparticles and surface morphologies of the (e) Kapton layer.

conformal layer of Ni nanoparticles (see Figure 1d), while the surface of the Kapton film is relatively smooth (see Figure 1e). The nanoscale roughness of the Ni film would be helpful for the energy generation due to the larger contact surface area during contact electrification.[38] The resistance of a Ni belt (1.5 cm × 20 cm) is measured to be about 2 Ω.

The working principle of the WTENG-flag is schematically depicted in Figure 2a. Each woven unit is a stack of KSC belts and Ni belts, and the two belts are not tightly woven to leave a space between. The wind-driven fluttering of the WTENG-flag will then lead to the relative contact-separation motion between the KSC belt and Ni belt. The unit stack can be treated as an arch with a gap between (see Figure 2a). At the original state without wind blowing, there is no charge transferred (see Figure 2a,i). Once the wind-introduced vibration of the WTENG-flag brings the KSC belt and Ni belt into full contact (see Figure 2a,ii), electrification of the Kapton film occurs by capturing electrons from the tribo-positive Ni film,[39,40] resulting in the negatively charged KSC belt and positively charged Ni belt. When the KSC belt and Ni belt are separated, a potential between the Ni belt and the Cu sandwiched inside the KSC belt will be generated. At short-circuit conditions, the electrostatic induction by the negative Kapton film drives the electron transfer from the Cu to the Ni belt through the external circuit, yielding an output current pulse (see Figure 2a,iii). When the KSC belt and Ni belt move together again, a current pulse with opposite direction will be generated. The wind-driven vibration of the unit stacks of KSC belts and Ni belts will then lead to the repetitive contact-separation motions and therefore alternative current pulses.[41] The open-circuit voltage (V_{oc}) and rectified short-circuit current (I_{sc}) are presented in Figure 2b,c, respectively. The output performances

DOI: 10.1021/acsnano.5b07157
ACS Nano XXXX, XXX, XXX−XXX

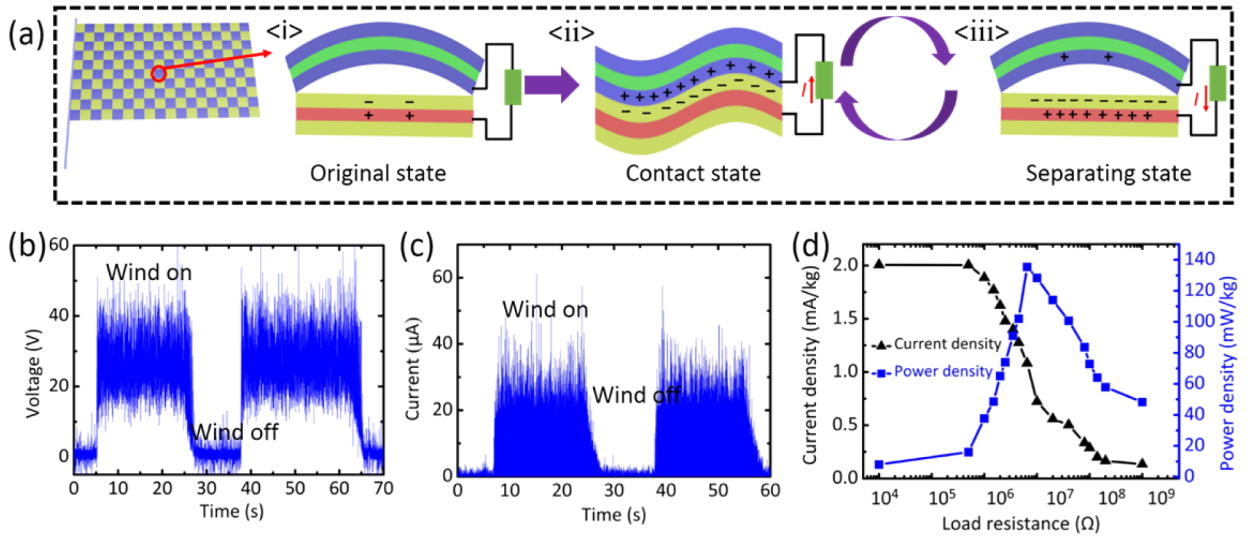

Figure 2. (a) Schematic illustration of working principle of the WTENG-flag: (i) Original state of the arch-shaped TENG without wind blowing. (ii) Wind force brings the KSC belt and Ni belt into full surface contact, generating positive triboelectric charges on the Ni belt and negative charges on the KSC belt. An electric potential difference is produced between the two electrodes; as a consequence, the charges were driven from the Cu electrode of KSC to the Ni cloth. (iii) Withdrawal of the wind force causes a separation. Potential difference drives positive charges from the Ni belt to the KSC belt until the potential difference is fully offset by the transferred charges. (b) Output open-circuit voltage. (c) Output rectified short-circuit current. (d) Variation of current and power of the WTENG-flag with external load resistances and the output performances of the WTENG-flag (the woven unit is 1.5 × 1.5 cm, and the degree of tightness is 1.09) were measured at a wind speed of 22 m/s.

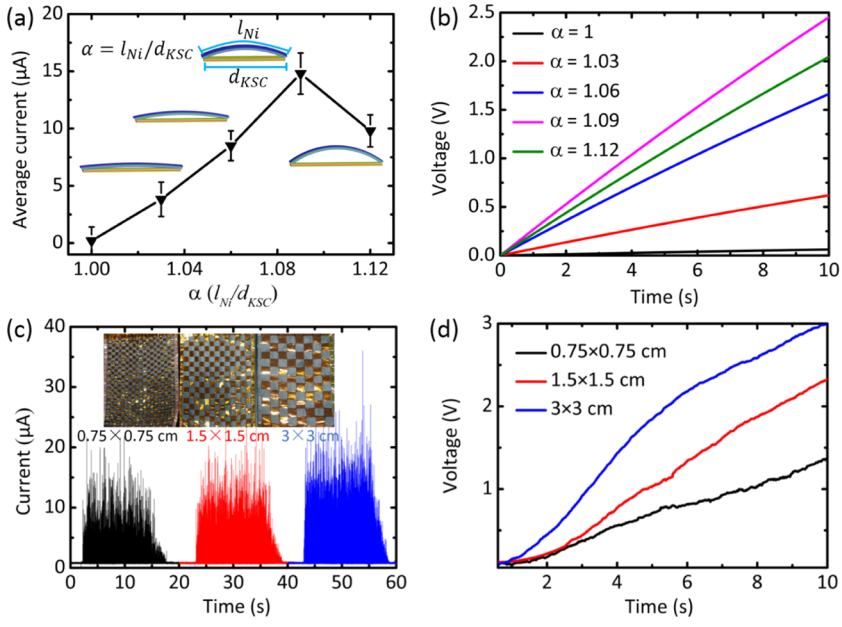

Figure 3. Output average rectified short-circuit current (a) and charging rate for a 4.7 μF capacitor (b) with different degrees of tightness varying from 1 to 1.12. (c) Dependence of rectified short-circuit current of the WTENG-flag on the size of woven unit; the inset is the photograph of the WTENG-flags with different sizes of woven unit, *i.e.*, 0.75 × 0.75 cm, 1.5 × 1.5 cm, 3 × 3 cm. (d) Charging rate for a 4.7 μF capacitor with different sizes of woven unit at the same time interval. The performances of WTENG-flags (the degree tightness is 1.09) were measured at a wind speed of 14 m/s.

of WTENG-flag (the woven unit is 1.5 × 1.5 cm, and the degree of tightness is 1.09) were measured at the wind speed of 22 m/s. As the vibration of all the woven unit stacks are not in resonance, large variation of the voltage and current is observed. The maximum V_{oc} and I_{sc} is about ∼40 V and ∼30 μA, respectively, which is dramatically improved compared with a previously reported flutter-driven wind TENG.[15,33] To further improve the output current/voltage of the WTENG, the following methods can be considered: (1) having nanoscale surface roughness of the polymer film to increase the contact surface area; (2) modification of the surface of the polymer film with more tribo-negative functional groups (such as fluorine-containing molecules) to improve the charge density by contact electrification.

In order to measure the output power of the WTENG-flag, external load resistances are connected with the WTENG-flag

DOI: 10.1021/acsnano.5b07157
ACS Nano XXXX, XXX, XXX−XXX

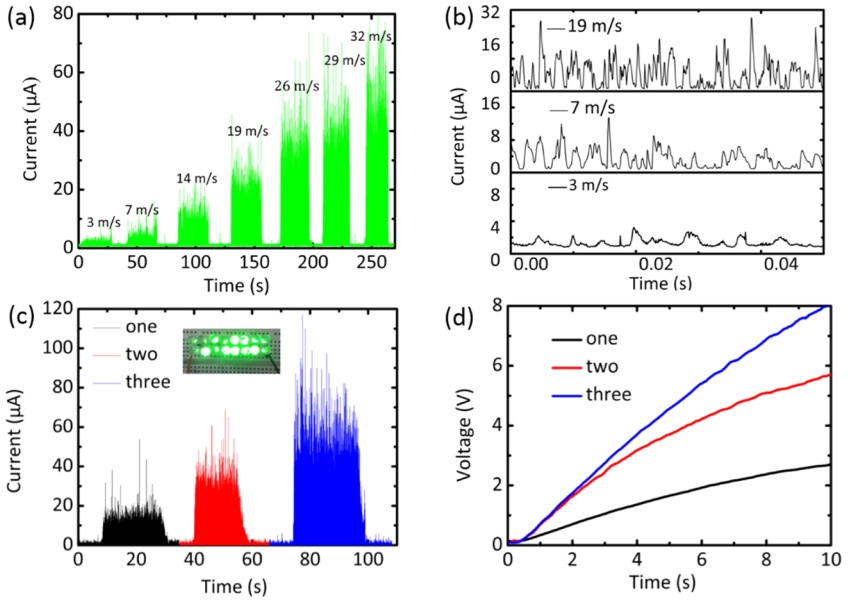

Figure 4. Rectified short-circuit current (a) and electric current frequency peak (b) as a function of various wind speeds. (c) Rectified short-circuit current of different numbers of WTENG-flags connected in parallel; the inset is photograph that lights up 16 green LEDs brightly with three WTENG-flags connected in parallel. (d) Charging rate for a 4.7 μF capacitor charged by different numbers of WTENG-flags connected in parallel. The output performances of WTENG-flags (the woven unit is 1.5 × 1.5 cm, and the degree of tightness is 1.09) were measured at a wind speed of 14 m/s.

ranging from 10 KΩ to 100 MΩ. The average peak current shows no obvious decrease until the external load resistance increases to 1 MΩ, indicating that the WTENG-flag is suitable for a constant current source.[42] When the external load resistances are continually increased, the output current significantly drops, as shown in Figure 2d. The instantaneous output power density is calculated by $P = (I^2R)/W$, where I is the output current, R is the load resistance, and W is the weight of the WTENG-flag. The maximum value of the output peak power density reaches 135 mW/kg at the resistance of 6.5 MΩ.

As the electricity generation of the WTENG-flag is realized by the relative contact-separation motions between the KSC belt and Ni belt in each woven unit, the gap distance, or the tightness of the woven flag, is an important parameter affecting the output of the WTENG-flag. We defined $\alpha = l_{Ni}/d_{KSC}$ to describe the degree of tightness, where l_{Ni} is the length of the Ni belt in each stacking unit and d_{KSC} is the width of the KSC belt. $\alpha = 1$ means that the flag is tightly woven and that no gap is left; $\alpha > 1$ means that there is a gap in the unit stack, and larger α means the larger gap distance. As shown in Figure 3a, almost no current was generated at $\alpha = 1$ when the wind speed was 14 m/s. An optimum current output of 15 μA was achieved by increasing α to 1.09. Further increasing the α to 1.12, that is, using a loosely woven flag, results in the decrease of the output current to 10 μA. It is easy to understand that the KSC belts and Ni belts can be woven neither too tightly nor too loosely because, in both cases, the contact-separation motions between the KSC belts and Ni belts in a woven unit will be hard to achieve. This effect was further confirmed by charging a 4.7 μF capacitor with the WTENG-flag with different degree of tightness. Fastest charging rate was achieved by the WTENG-flag with the optimized α (1.09), as shown in Figure 3b.

An investigation of the effect of the size of the woven unit on the output performances was also carried out. We varied the size of the woven unit (*i.e.*, 0.75 × 0.75 cm, 1.5 × 1.5 cm, 3 × 3 cm) and kept the wind speed (14 m/s), degree of tightness (α = 1.09), and the total flag area the same for all three conditions. A positive dependence of the output current on the woven unit size was observed, as shown in Figure 3c. Comparing the WTENG-flag with a smaller unit size, the WTENG-flag with a larger unit size shows higher amplitude of short-circuit current (see Figure 3c) and a higher charging rate of a 4.7 μF capacitor (see Figure 3d). As mentioned above, the vibration of the woven unit in a flag is not in resonance; therefore, some woven units are vibrating to separate when some others are vibrating to contact, which will neutralize the charge transfer and result in a smaller net current. We believe that increasing the unit size, that is, decreasing the number of woven units in the same area, will decrease the chances of charge neutralization and increase the net output current.

Wind at high altitude is faster and more consistent than that near the ground, and wind energy significantly increases with an increasing altitude.[5] Therefore, it is necessary to investigate the electric output of the WTENG-flag as a function of the wind speed. A systematic measurement was performed with different wind speeds ranging from 3 to 32 m/s. Figure 4a is the rectified short-circuit current as a function of wind speeds. It can be seen obviously that the rectified short-circuit current substantially increases with the wind speeds. We also summarized the fluttering frequency of the WTENG-flag under different wind speeds by counting the number of current peaks at the same time interval (0.05 s). A higher wind speed causes a more frequent fluttering of the WTENG-flag and thus results in the higher current frequencies, as shown in Figure 4b. The relationship between higher wind speed and larger current amplitude is due to larger wind force and shorter contact time. A larger wind force will enhance the effective contact area between the KSC belts and Ni belts, resulting in a higher surface charge density.[43] Therefore, from the equation $I = dQ/dt$, larger current amplitude is achieved by transferring more charges in shorter time at higher fluttering frequency. The peak power density with various wind speeds is summarized in

DOI: 10.1021/acsnano.5b07157
ACS Nano XXXX, XXX, XXX−XXX

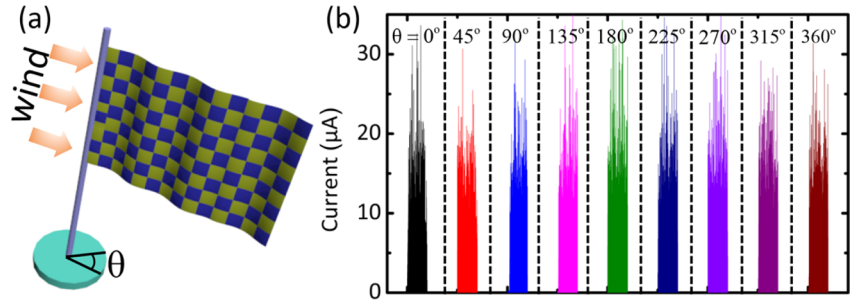

Figure 5. (a) Schematic illustration of the WTENG-flag with various incident angles of wind. (b) Output current of the WTENG-flag with various incident angles of wind from 0 to 360°. The output performances of WTENG-flag (the woven unit is 3 × 3 cm, and the degree of tightness is 1.09) were measured at a wind speed of 14 m/s.

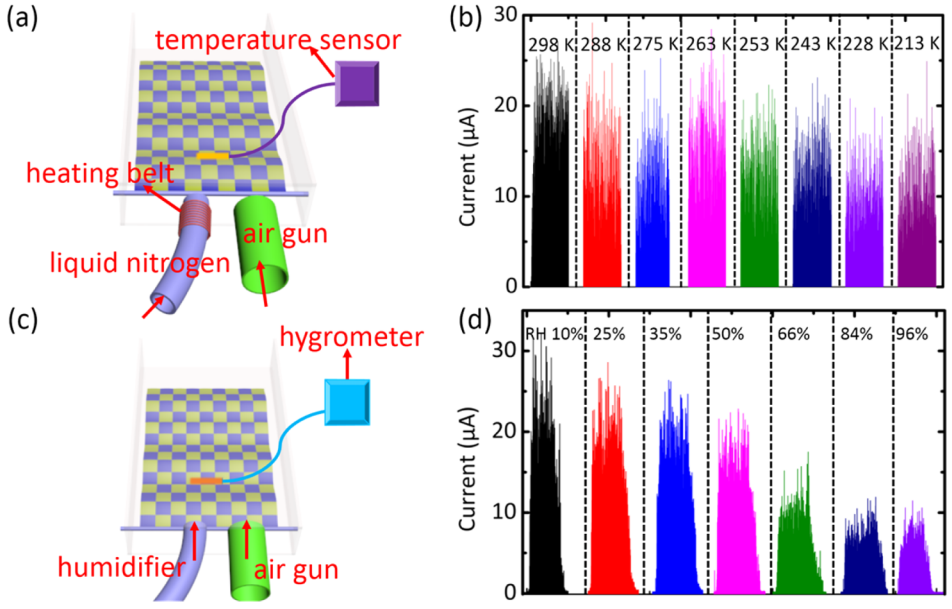

Figure 6. Effects of temperature and humidity on the performances of the WTENG-flag. Schematic illustration of the experimental setup for measuring the output current of a WTENG-flag at different temperature (a) and humidity (c). The measured output currents of a WTENG-flag at various temperatures (b) and relative humidities (d). The above output performances of WTENG-flag (the woven unit is 3 × 3 cm, and the degree of tightness is 1.09) were measured at a wind speed of 14 m/s.

Figure S2. The power density also increases with the wind speeds, suggesting the possible higher output at elevated altitude, where the wind is faster. Meanwhile, the stability of the WTENG-flag was evaluated by testing the output current about 2 months after its initial fabrication, as shown in Figure S3. The output current 2 months later is almost the same as that at the initial stage.

Because our WTENG-flag is a 2D design, it is facile to stack many flags together in parallel connections to increase the output current. To demonstrate this scale-up capability, we connected three WTENG-flags in parallel and measured the rectified short-circuit current, as shown in Figure 4c. The current amplitudes are nearly doubled or tripled for two or three WTENG-flags in parallel, respectively, suggesting a good linearity between the output and the number of flags (see Figure 4c). Meanwhile, the three flags connected in parallel can light up 16 green commercial LEDs brightly, as shown by the inset of Figure 4c. The charging rate of a 4.7 μF capacitor by different numbers of WTENG-flags connected in parallel is shown in Figure 4d. At the same time interval (about 10 s), the measured voltage (8.1 V) of a 4.7 μF capacitor charged by three WTENG-flags in parallel is about 3 times that of one WTENG-flag (2.7 V), further confirming that many flags can be stacked together for an almost linearly increased output.

For previously reported flutter-driven TENGs,[35,36] the flag is confined inside a tube or case; therefore, the wind has to blow along the axis of the tube or case for energy harvesting. Extra mechanisms are required to adjust the TENG according to the wind direction in real applications. This limitation was overcome by our design. Since our WTENG-flag is a freestanding 2D design, the flag can adjust itself according to the wind directions, leading to the capability of energy harvesting of wind from arbitrary directions. This is of key importance since the wind in the natural world is usually astatic. An experimental demonstration was carried out by blowing wind from various incident angles, as schemed in Figure 5a. Corresponding output short currents of the WTENG with various incident angles of wind are summarized in Figure 5b. No obvious difference in the amplitude of the current is observed with different incident angles ranging from 0 to 360°. Furthermore, as shown in Video S1, the WTENG-flag can keep lighting up 10 green LEDs when changing the wind directions, confirming the wind-direction-independent energy harvesting of the WTENG.

DOI: 10.1021/acsnano.5b07157
ACS Nano XXXX, XXX, XXX−XXX

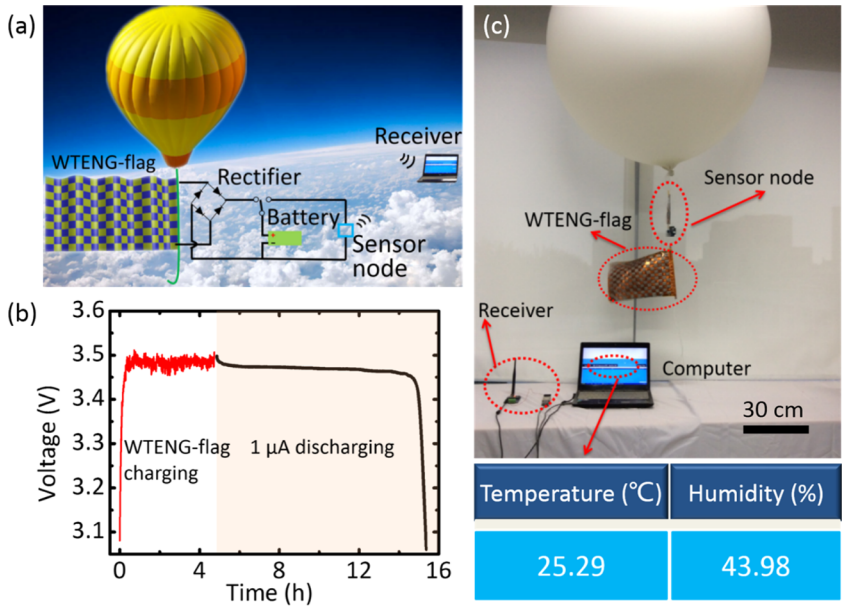

Figure 7. Demo of WTENG-flag for harvesting high-altitude wind energy and powering wireless temperature and humidity sensor node. (a) Equivalent electric circuit of the self-powered wireless temperature and humidity sensor node. (b) Voltage profiles of the button battery charged by WTENG-flag and galvanostatically discharged (GD) at 1 μA. (c) Optical image of the integrated self-powered system that harvests wind energy with WTENG-flag, stores the energy with button battery, and powers wireless temperature and humidity sensor node, which has remote telecommunication with a computer.

Environmental effects must be considered for harnessing wind energy, especially for application of HAPs, which usually situate in the stratosphere (10−50 km altitude). Wind energy is stronger and more stable at high altitude, but the temperature also decreases with an increasing altitude in the troposphere; in the stratosphere, the temperature increases with the altitude, reaching about 270 K (−3 °C) at the top layer of the stratosphere.[44] Meanwhile, the humidity in the stratosphere is much smaller than that near the ground. Therefore, experiments were conducted to evaluate the performances of the WTENG in a harsh environment at low temperatures and at various relative humidities (RH), as schemed in Figure 6a,c, respectively. The WTENG was confined in a case where liquid nitrogen and a heating belt were used together to control the temperature (Figure 6a). When varying the relative humidity, a commercial humidifier was utilized to increase the humidity (Figure 6c). The optical photos of the experimental setups are shown in Figure S4. The output current of the WTENG-flag at various temperatures from 298 to 213 K is shown in Figure 6b. At room temperature (298 K), the average current is about 16 μA. When the temperature is decreased, the current amplitude shows almost no decrease until reaching 263 K. However, even at the low temperature of 213 K, the WTENG-flag still maintains high output current (about 11 μA). This is consistent with the experiment by Wen *et al.*,[45,46] where a very slight decrease in output current can be observed at low temperature. Figure 6d shows the output current of the WTENG-flag at various relative humidity from 10 to 96%. It can be seen clearly that the output current decreases with increasing humidity. In a very dry environment (RH 10%), the output current can be up to 22 μA; in a highly wet environment (RH 96%), the WTENG can still work but the current sharply decreases to 8 μA. This humidity dependency is mainly due to the Kapton we used in the WTENG is slightly hydrophilic. The adsorption of the water vapor on the Kapton/Ni surface can reduce charges generated by the contact electrification or can discharge the surface.[47] The effect of the humidity, however, can be alleviated or eliminated by using hydrophobic materials (such as polytetrafluoroethylene).[45,48] Therefore, the WTENG-flag is suitable for high-altitude applications in the stratosphere with low temperature and low humidity; meanwhile, it can also work near the ground over a wide range of environmental conditions.

The WTENG-flag is an ideal energy supplier for self-powered HAPs without battery recharging or fuel refilling because it is lightweight, freestanding, and independent of the wind directions. Considering its pulsed output, an energy storage device is still needed to store the harvested wind energy and provide constant power supply for sensors or monitors in a HAP. We designed a demo of a self-powered and small-scale HAP with wireless temperature and humidity sensor node, as shown by the equivalent electric circuit in Figure 7a. The current generated by the WTENG-flag was rectified to charge a battery and then to power a sensor node which has wireless communication with a computer. This system could be potentially applied in a meteorological balloon for collecting information on temperature, humidity, *etc.* A homemade button battery was fabricated with $LiFePO_4$ as the cathode and Li as the anode. We charged the button battery with the WTENG-flag at a wind speed of 14 m/s for 4.8 h, which later showed an operational voltage of about 3.5 V and delivered a discharge capacity of 10 μAh at a discharge current of 1 μA (see Figure 7b). This charged button battery can power the temperature and humility sensor node, whose working voltage and current is about 3.5 V and 10 μA, respectively. Figure 6c shows the whole system fabricated in the laboratory. The WTENG-flag and sensor node were hung under the meteorological balloon; the temperature and humidity were then sent to the remote receiver and displayed on the computer. For the indoor room condition, the measured temperature and humidity were 25.29 °C and 43.98%, respectively (see the inset in Figure 7c). Video S2 (see Supporting Information) also shows the measured temperature and humidity information on the sensor node,

DOI: 10.1021/acsnano.5b07157
ACS Nano XXXX, XXX, XXX−XXX

which is powered by a freestanding WTENG-flag and is of great potential in applications in self-powered HAPs for weather/environmental monitoring.

CONCLUSION

In summary, we have developed an innovative WTENG-flag that can harness high-altitude wind energy of arbitrary directions. This freestanding nanogenerator was demonstrated to be capable of converting the wind-driven fluttering of the woven units of the flag into electricity. The effects of the degree of tightness and unit size of the WTENG-flag were investigated to optimize the output current. By increasing the wind speeds, the output current increases linearly and power density is enhanced exponentially. Meanwhile, our 2D WTENG-flags can be stacked in parallel connections for many layers for a linearly increased output. The suitability of the WTENG-flag for a wide range of environmental conditions was also confirmed, especially for low temperature and low humidity at high altitude. Lastly, a self-powered temperature and humidity sensor node with wireless communication to a remote computer was demonstrated by using a power supply system with the WTENG-flag as the wind energy harvester and a button battery for the energy storage. Considering the light weight, low cost, and easy scale-up, our WTENG-flag is of great potential in applications such as weather/environmental sensing/monitoring systems.

EXPERIMENTAL METHODS

Preparation of the WTENG-Flag. The conductive Ni cloth textile was synthesized by an electroless plating of Ni on the original polyester cloth. The pristine cloth was cleaned with DI water and acetone by an ultrasonic cleaner. Subsequently, it was soaked into the solution of 10 g L^{-1} $SnCl_2$ and 40 mL L^{-1} 38% HCl and then immersed into aqueous solution of 0.5 g L^{-1} $PdCl_2$ and 20 mL L^{-1} 38% HCl at room temperature for 10 min, respectively. After being washed in DI water, the seeded polyester cloth was immersed into aqueous solution of 0.1 M $NiSiO_4$ (whose pH was adjusted to 10 by adding 10% NaOH solution) for coating Ni at 80 °C for 10 min. After the coating, the Ni cloth was cleaned with DI water and dried in a vacuum oven. The KSC belts were obtained by sealing both sides of the Cu foil with the Kapton film (20 μm thick). The WTENG-flag was woven with 18 Ni cloth belts (20 cm) as longitude lines and 12 sandwiched KSC belts (30 cm) as latitude lines. All Ni belts were connected by copper tape as one electrode, and all sandwiched KSC belts were connected as the other electrode.

Characterizations and Measurements. For the measurements of the WTENG-flag, wind was applied by a commercial air gun, and wind speed was measured *via* a commercial anemometer. The output short-circuit current and open-circuit voltage of the WTENG-flag were measured by a Stanford low-noise current preamplifier (model SR570) and a Keithley electrometer (Keithley 6514), respectively. The charge and discharge profiles of the button battery were recorded by Keithley 6514 and LANDCT2001A, respectively. A temperature and humidity sensor was used in the HAP demo as the wireless sensor node, and the power consumption of the whole system, including the wireless signal launch, was less than 100 μW.

ASSOCIATED CONTENT

Supporting Information

The Supporting Information is available free of charge on the ACS Publications website at DOI: 10.1021/acsnano.5b07157.

Figures S1–S4 (PDF)
Video S1 (AVI)
Video S2 (AVI)

AUTHOR INFORMATION

Corresponding Authors

*E-mail: huweiguo@binn.cas.cn.
*E-mail: zlwang@gatech.edu.

Author Contributions

§Z.Z. and X.P. contributed equally to this work.

Notes

The authors declare no competing financial interest.

ACKNOWLEDGMENTS

The authors acknowledge the support from the "thousands talents" program for pioneer researcher and his innovation team, China, National Natural Science Foundation of China (Grant Nos. 51432005 and 61574018).

REFERENCES

(1) Herbert, G. M. J.; Iniyan, S.; Sreevalsan, E.; Rajapandian, S. A Review of Wind Energy Technologies. *Renewable Sustainable Energy Rev.* **2007**, *11*, 1117–1145.
(2) Ackermann, T.; Soder, L. Wind Energy Technology and Current Status: A Review. *Renewable Sustainable Energy Rev.* **2000**, *4*, 315–374.
(3) Perkovic, L.; Silva, P.; Ban, M.; Kranjcevic, N.; Duic, N. Harvesting High Altitude Wind Energy for Power Production: The Concept Based on Magnus' Effect. *Appl. Energy* **2013**, *101*, 151–160.
(4) Adhikari, J.; Panda, S. K.; Rathore, A. K. Harnessing High Altitude Wind Power Using Light Gas Filled Blimp. *IEEE. Ind. Elec.* **2013**, 7163–7168.
(5) Roberts, B. W.; Shepard, D. H.; Caldeira, K.; Cannon, M. E.; Eccles, D. G.; Grenier, A. J.; Freidin, J. F. Harnessing High-Altitude Wind Power. *IEEE. T. Energy.Conver.* **2007**, *22*, 136–144.
(6) Canale, M.; Fagiano, L.; Milanese, M. Power Kites for Wind Energy Generation Fast Predictive Control of Tethered Airfoils. *IEEE. Contr. Syst. Mag.* **2007**, *27*, 25–38.
(7) Archer, C. L.; Caldeira, K. Global Assessment of High-Altitude Wind Power. *Energies* **2009**, *2*, 307–319.
(8) Widiawan, A. K.; Tafazolli, R. High Altitude Platform Station (HAPS): A Review of New Infrastructure Development for Future Wireless Communications. *Wireless. Pers. Commun.* **2007**, *42*, 387–404.
(9) Avagnina, D.; Dovis, F.; Ghiglione, A.; Mulassano, P. Wireless Networks Based on High-Altitude Platforms for the Provision of Integrated Navigation/Communication Services. *IEEE. Commun. Mag.* **2002**, *40*, 119–125.
(10) Watts, A. C.; Ambrosia, V. G.; Hinkley, E. A. Unmanned Aircraft Systems in Remote Sensing and Scientific Research: Classification and Considerations of Use. *Remote. Sens.Basel.* **2012**, *4*, 1671–1692.
(11) Berni, J. A. J.; Zarco-Tejada, P. J.; Suarez, L.; Fereres, E. Thermal and Narrowband Multispectral Remote Sensing for Vegetation Monitoring From an Unmanned Aerial Vehicle. *IEEE. T. Geosci. Remote.* **2009**, *47*, 722–738.
(12) Ockels, W. J. Laddermill, A Novel Concept to Exploit the Energy in the Airspace. *Aircraft design* **2001**, *4*, 81–97.
(13) Williams, P.; Lansdorp, B.; Ockesl, W. Optimal Crosswind Towing and Power Generation with Tethered Kites. *J. Guid. Control. Dynam.* **2008**, *31*, 81–93.
(14) Lee, S.; Ko, W.; Oh, Y.; Lee, J.; Baek, G.; Lee, Y.; Sohn, J.; Cha, S.; Kim, J.; Park, J.; Hong, J. Triboelectric Energy Harvester Based on Wearable Textile Platforms Employing Various Surface Morphologies. *Nano Energy* **2015**, *12*, 410–418.
(15) Seol, M.-L.; Woo, J.-H.; Jeon, S.-B.; Kim, D.; Park, S.-J.; Hur, J.; Choi, Y.-K. Vertically Stacked Thin Triboelectric Nanogenerator for Wind Energy Harvesting. *Nano Energy* **2015**, *14*, 201–208.
(16) Seung, W.; Gupta, M. K.; Lee, K. Y.; Shin, K. S.; Lee, J. H.; Kim, T. Y.; Kim, S.; Lin, J.; Kim, J. H.; Kim, S. W. Nanopatterned Textile-Based Wearable Triboelectric Nanogenerator. *ACS Nano* **2015**, *9*, 3501–3509.

DOI: 10.1021/acsnano.5b07157
ACS Nano XXXX, XXX, XXX–XXX

(17) Cheng, X. L.; Meng, B.; Zhang, X. S.; Han, M. D.; Su, Z. M.; Zhang, H. X. Wearable Electrode-Free Triboelectric Generator for Harvesting Biomechanical Energy. *Nano Energy* **2015**, *12*, 19−25.
(18) Liang, Q. J.; Yan, X. Q.; Gu, Y. S.; Zhang, K.; Liang, M. Y.; Lu, S. N.; Zheng, X.; Zhang, Y. Highly Transparent Triboelectric Nanogenerator for Harvesting Water-Related Energy Reinforced by Antireflection Coating. *Sci. Rep.* **2015**, *5*, 9080.
(19) Shin, S. H.; Kwon, Y. H.; Kim, Y. H.; Jung, J. Y.; Lee, M. H.; Nah, J. Triboelectric Charging Sequence Induced by Surface Functionalization as a Method To Fabricate High Performance Triboelectric Generators. *ACS Nano* **2015**, *9*, 4621−4627.
(20) Pu, X.; Liu, M.; Li, L.; Zhang, C.; Pang, Y.; Jiang, C.; Shao, L.; Hu, W.; Wang, Z. L. Efficient Charging of Li-Ion Batteries with Pulsed Output Current of Triboelectric Nanogenerators. *Adv. Sci.* **2015**, DOI: 10.1002/advs.201500255.
(21) He, X. M.; Guo, H. Y.; Yue, X. L.; Gao, J.; Xi, Y.; Hu, C. G. Improving Energy Conversion Efficiency for Triboelectric Nanogenerator with Capacitor Structure by Maximizing Surface Charge Density. *Nanoscale* **2015**, *7*, 1896−1903.
(22) Chandrashekar, B. N.; Deng, B.; Smitha, A. S.; Chen, Y. B.; Tan, C. W.; Zhang, H. X.; Peng, H. L.; Liu, Z. F. Roll-to-Roll Green Transfer of CVD Graphene onto Plastic for a Transparent and Flexible Triboelectric Nanogenerator. *Adv. Mater.* **2015**, *27*, 5210−5216.
(23) Kim, D.; Jeon, S. B.; Kim, J. Y.; Seol, M. L.; Kim, S. O.; Choi, Y. K. High-Performance Nanopattern Triboelectric Generator by Block Copolymer Lithography. *Nano Energy* **2015**, *12*, 331−338.
(24) Lee, K. Y.; Chun, J.; Lee, J. H.; Kim, K. N.; Kang, N. R.; Kim, J. Y.; Kim, M. H.; Shin, K. S.; Gupta, M. K.; Baik, J. M.; Kim, S. W. Hydrophobic Sponge Structure-Based Triboelectric Nanogenerator. *Adv. Mater.* **2014**, *26*, 5037−5042.
(25) Tang, W.; Meng, B.; Zhang, H. X. Investigation of Power Generation Based on Stacked Triboelectric Nanogenerator. *Nano Energy* **2013**, *2*, 1164−1171.
(26) Xie, Y. N.; Wang, S. H.; Niu, S. M.; Lin, L.; Jing, Q. S.; Yang, J.; Wu, Z. Y.; Wang, Z. L. Grating-Structured Freestanding Triboelectric-Layer Nanogenerator for Harvesting Mechanical Energy at 85% Total Conversion Efficiency. *Adv. Mater.* **2014**, *26*, 6599−6607.
(27) Hinchet, R.; Kim, S. W. Wearable and Implantable Mechanical Energy Harvesters for Self-Powered Biomedical Systems. *ACS Nano* **2015**, *9*, 7742−7745.
(28) Meng, B.; Tang, W.; Too, Z. H.; Zhang, X. S.; Han, M. D.; Liu, W.; Zhang, H. X. A Transparent Single-Friction-Surface Triboelectric Generator and Self-Powered Touch Sensor. *Energy Environ. Sci.* **2013**, *6*, 3235−3240.
(29) Zhong, J. W.; Zhu, H. L.; Zhong, Q. Z.; Dai, J. Q.; Li, W. B.; Jang, S. H.; Yao, Y. G.; Henderson, D.; Hu, Q. Y.; Hu, L. B.; Zhou, J. Self-Powered Human-Interactive Transparent Nanopaper Systems. *ACS Nano* **2015**, *9*, 7399−7406.
(30) Pu, X.; Li, L.; Song, H.; Du, C.; Zhao, Z.; Jiang, C.; Cao, G.; Hu, W.; Wang, Z. L. A Self-Charging Power Unit by Integration of a Textile Triboelectric Nanogenerator and a Flexible Lithium-Ion Battery for Wearable Electronics. *Adv. Mater.* **2015**, *27*, 2472−2478.
(31) Pu, X.; Li, L.; Liu, M.; Jiang, C.; Du, C.; Zhao, Z.; Hu, W.; Wang, Z. L. Wearable Self-Charging Power Textile Based on Flexible Yarn Supercapacitors and Fabric Nanogenerators. *Adv. Mater.* **2016**, *28*, 98.
(32) Bai, P.; Zhu, G.; Jing, Q. S.; Yang, J.; Chen, J.; Su, Y. J.; Ma, J. S.; Zhang, G.; Wang, Z. L. Membrane-Based Self-Powered Triboelectric Sensors for Pressure Change Detection and Its Uses in Security Surveillance and Healthcare Monitoring. *Adv. Funct. Mater.* **2014**, *24*, 5807−5813.
(33) Guo, H. Y.; He, X. M.; Zhong, J. W.; Zhong, Q.; Leng, Q.; Hu, C. G.; Chen, J.; Tian, L.; Xi, Y.; Zhou, J. A Nanogenerator for Harvesting Airflow Energy and Light Energy. *J. Mater. Chem. A* **2014**, *2*, 2079−2087.
(34) Wang, S.; Mu, X.; Yang, Y.; Sun, C.; Gu, A. Y.; Wang, Z. L. Flow-Driven Triboelectric Generator for Directly Powering a Wireless Sensor Node. *Adv. Mater.* **2015**, *27*, 240−248.
(35) Meng, X. S.; Zhu, G.; Wang, Z. L. Robust Thin-Film Generator Based on Segmented Contact-Electrification for Harvesting Wind Energy. *ACS Appl. Mater. Interfaces* **2014**, *6*, 8011−8016.
(36) Bae, J.; Lee, J.; Kim, S.; Ha, J.; Lee, B. S.; Park, Y.; Choong, C.; Kim, J. B.; Wang, Z. L.; Kim, H. Y.; Park, J. J.; Chung, U. Flutter-Driven Triboelectrification for Harvesting Wind Energy. *Nat. Commun.* **2014**, *5*, 4929.
(37) Xie, Y. N.; Wang, S. H.; Lin, L.; Jing, Q. S.; Lin, Z. H.; Niu, S. M.; Wu, Z. Y.; Wang, Z. L. Rotary Triboelectric Nanogenerator Based on a Hybridized Mechanism for Harvesting Wind Energy. *ACS Nano* **2013**, *7*, 7119−7125.
(38) Chun, J.; Kim, J. W.; Jung, W. S.; Kang, C. Y.; Kim, S. W.; Wang, Z. L.; Baik, J. M. Mesoporous Pores Impregnated with Au Nanoparticles as Effective Dielectrics for Enhancing Triboelectric Nanogenerator Performance in Harsh Environments. *Energy Environ. Sci.* **2015**, *8*, 3006−3012.
(39) Wang, S.; Lin, L.; Wang, Z. L. Nanoscale Triboelectric-Effect-Enabled Energy Conversion for Sustainably Powering Portable Electronics. *Nano Lett.* **2012**, *12*, 6339−6346.
(40) Diaz, A. F.; Felix-Navarro, R. M. A Semi-Quantitative Triboelectric Series for Polymeric Materials: The Influence of Chemical Structure and Properties. *J. Electrost.* **2004**, *62*, 277−290.
(41) Niu, S. M.; Liu, Y.; Wang, S. H.; Lin, L.; Zhou, Y. S.; Hu, Y. F.; Wang, Z. L. Theoretical Investigation and Structural Optimization of Single-Electrode Triboelectric Nanogenerators. *Adv. Funct. Mater.* **2014**, *24*, 3332−3340.
(42) Zhang, C.; Tang, W.; Han, C. B.; Fan, F. R.; Wang, Z. L. Theoretical Comparison, Equivalent Transformation, and Conjunction Operations of Electromagnetic Induction Generator and Triboelectric Nanogenerator for Harvesting Mechanical Energy. *Adv. Mater.* **2014**, *26*, 3580−3591.
(43) Zhu, G.; Lin, Z. H.; Jing, Q. S.; Bai, P.; Pan, C. F.; Yang, Y.; Zhou, Y. S.; Wang, Z. L. Toward Large-Scale Energy Harvesting by a Nanoparticle-Enhanced Triboelectric Nanogenerator. *Nano Lett.* **2013**, *13*, 847−853.
(44) Seinfeld, J. H.; Pandis, S. N. *Atmospheric Chemistry and Physics: From Air Pollution to Climate Change*, 2nd ed.; Wiley: Hoboken, NJ, 2006.
(45) Nguyen, V.; Zhu, R.; Yang, R. S. Environmental Effects on Nanogenerators. *Nano Energy* **2015**, *14*, 49−61.
(46) Wen, X. N.; Su, Y. J.; Yang, Y.; Zhang, H. L.; Wang, Z. L. Applicability of Triboelectric Generator Over a Wide Range of Temperature. *Nano Energy* **2014**, *4*, 150−156.
(47) McCarty, L. S.; Whitesides, G. M. Electrostatic Charging Due to Separation of Ions at Interfaces: Contact Electrification of Ionic Electrets. *Angew. Chem., Int. Ed.* **2008**, *47*, 2188−2207.
(48) Lin, Z. H.; Cheng, G.; Lin, L.; Lee, S.; Wang, Z. L. Water-Solid Surface Contact Electrification and Its Use for Harvesting Liquid-Wave Energy. *Angew. Chem., Int. Ed.* **2013**, *52*, 12545−12549.

DOI: 10.1021/acsnano.5b07157
ACS Nano XXXX, XXX, XXX−XXX